Chemical-Picture-Based Modeling of Thermodynamic Properties of Dense Multicharged-Ion Plasmas Using the Superconfiguration Approach

P.A. Loboda, V.V. Popova, and **A.A. Shadrin***

RFNC-VNIITF, 13, Vasilyeva st., Snezhinsk, Russia, 456770

Received 15 November 2009, revised 30 November 2009, accepted 2 December 2009
Published online 3 December 2009

Key words Chemical picture, dense plasma, equation of state, shell effects.
PACS 31.15.Ar, 31.15.Bs, 51.30.+i, 62.50.+p

Using the chemical-picture representation of plasmas as a mixture of various ions and free electrons, a consistent description of thermodynamics of dense multicharged-ion plasmas is being developed that involves the effects of Coulomb non-ideality and degeneracy of plasma electrons; contribution of the excited ion states (on the base of the superconfiguration approach) that may exist under an appropriate truncation of ion energy spectra due to plasma effects; hard-sphere-model representation of the finite-volume effects of plasma ions with the model parameters (effective ion sizes) corresponding to superconfigurations yielding the greatest contribution to partition functions. We present the calculated data for average ionization, Grüneisen coefficient, and specific heat of aluminum and iron plasmas at temperatures of 0.03–3 keV and densities $10^{-3} - 5$ of their normal material densities. Calculated thermodynamic functions and shock Hugoniots are compared with other theoretical and experimental data.

1 Intoduction

Consistent modeling of thermodynamic properties of dense plasmas in the warm-dense-matter (WDM) domain — at temperatures $T \geq E_F$ (E_F — Fermi energy) and densities ρ about or lower than normal solid density ρ_0 — is still one of the challenging problems to be addressed. Such plasmas are produced from interactions of intense radiation fluxes and particle beams in numerous present-day experimental studies on high-energy-density physics (HEDP). Therefore, this problem receives much attention in the leading national laboratories running HEDP research. These plasmas are characterized by strong Coulomb interactions, partial degeneracy of plasma electrons, presence of internal degrees of freedom due to the atomic-shell structure of multielectron ions (shell effects), perturbations of bound ionic states by plasma microfields, and the finite-ion-volume effects at high plasma densities. The lack of systematic experimental data in this range of plasma parameters strongly impedes derivation of the first-principles and semiempirical Equation-of-State (EOS) models.

Though one can simulate dense-plasma EOS by using well-developed and practically conceivable cell models [1], those models intrinsically fail to represent self-consistent converse effect of inter-ionic Coulomb correlations on the equilibrium electron distribution in a cell and therefore on the total thermodynamic functions [2].

This, however, can be done within the framework of chemical-picture (CP) approach [2–4] enabling to consider Coulomb interactions between all the charged particles and obtain both appropriate direct corrections to EOS and the shift of ionization equilibrium. It is also worth noting that apart from its traditional application to low-density plasmas, the CP-approach admits extrapolation to reasonably nonideal dense gas and expanded-metal plasmas in the density range $0.1 \leq \rho/\rho_0 \leq 1$ [2] we are interested in.

Recently, P. Hakel et al. [4] developed a CP-model of nonideal plasmas allowing for strong coupling of charged particles with analytic fits obtained from the hypernetted-chain and Monte Carlo simulations [5] and finite ion sizes by using multicomponent hard-sphere model of Mansoori [6]. The contribution of the excited bound states

* Corresponding author: e-mail: A.A.Shadrin@vniitf.ru, Phone: +7 351 46 56560, Fax: +7 351 46 55118

of plasma ions was considered by using the detailed configuration accounting (DCA) approach with the plasma-microfields perturbations included by using the occupation-probability approximation [7].

In multielectron-ion plasmas, however, the number of excited ion states available under an appropriate truncation of ion energy spectra due to plasma effects may be enormous thus making an explicit implementation of the DCA approach almost untractable. The main goal of our effort is to develop a CP-model of dense multielectron-ion plasmas that would enable to reasonably treat manifolds of excited ion states by the grouping of energetically adjacent configurations into so-called superconfigurations [9–12] and appropriately include the effects of plasma non-ideality and degeneracy of plasma electrons. We present a description of the current version of the model along with the calculated results for average ionization, Grüneisen coefficient, and specific heat of aluminum and iron plasmas at temperatures of 0.03–3 keV and densities $10^{-3} - 5$ of their normal material densities. Calculated thermodynamic functions and shock Hugoniots are compared with other theoretical and experimental data.

2 A Chemical-Picture Model to calculate Thermodynamic Properties of Dense Multicharged-Ion Plasmas in the superconfiguration approximation

2.1 Free energy of Dense Multicharged-Ion Plasmas

It is well known that thermodynamically consistent relations for ionization and equation of state of a plasma as the functions of temperature and density under the conditions of local thermodynamic equilibrium (LTE) can be derived from the expression of the specific Helmholtz free energy of the plasma [2, 3, 8]:

$$F\left(\rho,T,\mathbf{N}\right)=\sum_{Q=0}^{Z}F_{Q}^{(id)}+F_{e}^{(id)}+\Delta F\left(\rho,T,\mathbf{N}\right),\quad \mathbf{N}=\{N_{Q},N_{e}\}. \tag{1}$$

Here,

$$F_{Q}^{(id)}=-N_{Q}k_{B}T\left(\ln\frac{\widetilde{U}_{Q}\left(\rho,T,\mathbf{N}\right)}{\rho N_{Q}\lambda^{3}}+1\right) \tag{2}$$

is the "ideal-gas" contribution of ions with Q bound electrons, abundant in the plasma at certain ρ and T, $N=\sum_{Q}N_{Q}=N_{A}/A$ — specific number of nuclei (per unit mass)[1]; Z — nuclear charge (atomic number); N_A — Avogadro number; N_Q and N_e — specific numbers of ions with the Q bound electrons and free electrons, respectively; $\lambda=\left(\beta h^{2}/\left(2\pi M\right)\right)^{1/2}$ — the thermal de Broglie wavelength of an ion with a mass $M=A/N_A$; k_B — Boltzmann constant; $\widetilde{U}_Q$ — modified internal partition function of a Q-electron ion that represents the contribution of bound-electron states perturbed by the plasma environment. The second term

$$F_{e}^{(id)}=-k_{B}TN_{e}\left(\frac{2}{3}\frac{I_{3/2}(X)}{I_{1/2}(X)}-X\right) \tag{3}$$

stands for the ideal-gas contribution of free electrons within partially degenerate Fermi-gas approximation, where $X=\beta\mu_{e}$; μ_e — chemical potential of free electrons; $I_k(X)$ — Fermi-Dirac integrals; $\beta=1/k_BT$; λ_e — the electron de Broglie wavelength.

Non-ideal contribution $\Delta F\left(\rho,T,\mathbf{N}\right)$ to the total Helmholtz free energy of the plasma takes into account Coulomb interaction of charged particles and finite-ion-volume effects. In order to cover a wide range of plasma conditions — both low-density, high-temperature regime and the strongly-coupled regime — we adopt the analytic fit of excess free energy of one-component plasma (OCP) of classical ions [5] generalized for multi-ionic mixture using the linear mixing rule (LMR):

$$\Delta F\left(\rho,T,\mathbf{N}\right)=Nk_{B}T\left[\sum_{Q}c_{Q}f_{C}(\Gamma)+f_{HS}\right], \tag{4}$$

[1] Here we restrict to the case of a plasma of one chemical element.

where $\Gamma = \Gamma_e \cdot \mathcal{Z}^{5/3}$ is the coupling parameter of $\mathcal{Z}$-charged ions, $\mathcal{Z} = Z - Q$; $\Gamma_e = \beta e^2/a_e$ is the electron coupling parameter with mean interelectron distance $a_e = (\frac{4}{3}\pi\rho N_e)^{-1/3}$, and

$$f_C(\Gamma) = A_1 \left[\sqrt{\Gamma(A_2+\Gamma)} - A_2 \ln\left(\sqrt{\Gamma/A_2} + \sqrt{1+\Gamma/A_2}\right)\right] + \\ +2A_3\left[\sqrt{\Gamma} - \arctan\sqrt{\Gamma}\right] + B_1\left[\Gamma - B_2 \ln\left(1+\frac{\Gamma}{B_1}\right)\right] + \frac{B_3}{2}\ln\left(1+\frac{\Gamma^2}{B_4}\right), \quad (5)$$

$A_1 = -0.907347$, $A_2 = 0.62849$, $B_1 = 4.5 \cdot 10^{-3}$, $B_2 = 170$, $B_3 = 8.4 \cdot 10^{-5}$, $B_4 = 3.7 \cdot 10^{-3}$, $A_3 = -\sqrt{3}/2 - A_1/\sqrt{A_2}$.

This fit is calculated from the OCP model via an interpolation between the Debye-Hückel limit and Abe correction for low-coupling conditions and Monte Carlo results for $\Gamma \geq 1$ [5]. The accuracy of the LMR for multicomponent strongly coupled Coulomb plasmas has been confirmed by H.E. DeWitt and coworkers [14–16].

Finite-ion-volume effects are approximately treated with the hard-sphere model [17]:

$$f_{HS}(\eta) = \frac{4\eta - 3\eta^2}{(1-\eta)^2}, \quad (6)$$

where $\eta = \sum_Q c_Q \left(\frac{R_Q}{a_i}\right)^3$ is the packing fraction; R_Q is the effective size of Q-electron ions; $a_i = (\frac{4}{3}\pi\rho N)^{-1/3}$ is the mean interionic distance.

2.2 Modified ion partition functions in the superconfiguration approximation

In the CP-approach, the contribution of bound-electron states to the free energy of dense multielectron-ion plasmas can be represented with the employment of superconfiguration (SC) approximation first introduced by A. Bar-Shalom and co-workers [9, 10] to formulate a Super-Transition-Array (STA) model for tractable description of complex emission and absorption spectra of such plasmas. In the SC-approximation, sets of ionic configurations of a Q-electron ion $\{C\}$,

$$C = (n_1 l_1 j_1)^{q_1} (n_2 l_2 j_2)^{q_2} \ldots (n_k l_k j_k)^{q_k} \equiv \prod_s^k (n_s l_s j_s)^{q_s} \quad (7)$$

(n_s, l_s, j_s stand for an s-subshell principal quantum number, orbital and total angular momenta, respectively), close in energy are gathered into superconfigurations defined as collections of supershells $\{\sigma\}$ — groups of energetically adjacent ionic subshells $\{n_s l_s j_s\}$ populated in all possible ways $\sum_{s\in\sigma} q_s = Q_\sigma$ consistent with the Pauli exclusion principle:

$$\Xi = \prod_\sigma \sigma^{Q_\sigma} \equiv \prod_\sigma \left(\prod_{s\in\sigma} n_s l_s j_s\right)^{Q_\sigma}, \qquad \sum_\sigma Q_\sigma = Q. \quad (8)$$

As a result, the number of SCs may be far less than the original number of ionic configurations. The main advantage of the SC-approximation lies in a possibility of providing a necessary level of detailing in the representation of bound-electron states. Thus, DCA approximation may readily be obtained as the most detailed variant of the SC-approximation with every SC being represented as a certain detailed configuration.

The SC-model is based on the assumption that in the LTE plasmas the Boltzmann factor is nearly constant within the ionic configurations so that detailed energy levels of a configuration may be considered as statistically populated. The population distribution amongst configurations within a SC is however considered to be the thermal one [9].

In the SC-approximation, average energies of configurations $\{C\}$ comprising a certain superconfiguration Ξ are represented as [9, 11]

$$E_C \approx E_C^{(0)} + \overline{\Delta E_\Xi}. \quad (9)$$

Here, $E_C^{(0)} = \sum_{s\in C} q_s\varepsilon_s$ is the zeroth-order configuration-average energy corresponding to the contribution of independent electrons with the energies ε_s found in the central potential of isolated Q-electron ion optimized for the configuration C. $\overline{\Delta E_\Xi}$ stands for the first-order average correction to $E_C^{(0)}$ common for all the configurations $\{C\} \in \Xi$ — an average of the energy difference $\left(E_C - E_C^{(0)}\right)_\Xi$.

Approximation (9) allows to explicitly detach the first-order contribution $\exp(-\beta\overline{\Delta E_\Xi})$ in the partition function of an SC:

$$U_\Xi = e^{-\beta\Delta E_\Xi} \cdot U_\Xi^{(0)}, \tag{10}$$

$$U_\Xi^{(0)} = \prod_{\sigma\in\,\Xi} U_\sigma = \sum_{\sum_s q_s = Q_\sigma} \prod_{s\in\,\sigma} \binom{g_s}{q_s} \cdot X_s^{q_s}, \quad X_s = e^{-\beta\varepsilon_s}. \tag{11}$$

The partition function of a Q-electron ion within the framework of the SC-approach is:

$$U_Q = \sum_\Xi U_\Xi. \tag{12}$$

Here, U_Ξ — partition function of a SC Ξ of Q-electron ion; $\{Q_\sigma\}$ — supershell occupation numbers; U_σ — partition function of supershell σ; q_s and ε_s — stand for occupation number (population) and one-electron energy of atomic shell s, respectively; $\binom{g_s}{q_s}$ — binomial coefficient and $g_s = (2j_s + 1)$ is the statistical weight (degeneracy) of the shell s.

One of the basic achievements of the SC-approach lies in the possibility to calculate supershell partition functions with recursion relations [10]:

$$Q_\sigma U_{Q_\sigma} = \sum_{i=0}^{Q_\sigma - 1} U_i\, \chi_{Q_\sigma - i}, \quad \chi_k = \sum_s \left(-g_s\,(-X_s)^k\right), \quad i < Q_\sigma, \quad U_0 = 1. \tag{13}$$

Thus, the partition function of a supershell with Q_σ bound electrons can be calculated at only Q_σ recursion loops.

However, the calculation of partition functions on the base of the SC-method using recursion relations (13) [9, 10] involves the alternating summation of large negative and positive numbers. This results in a strong numerical instability that can severely limit the range of applicability of the SC-model, in particular in the case of relatively low-temperature regime and/or when large supershells are considered, thus inhibiting the possibility of arranging arbitrary supershell gathering essential to the SC-model [12].

F. Gilleron and J.C. Pain [12] proposed a stable method to calculate partition functions of SCs with no restriction on thermodynamic conditions and gathering of supershells. In particular, new recursion relations, obtained by F. Gilleron and J.C. Pain, do not contain any alternating summation thus enabling one to avoid numerical difficulties due to the substraction of large numbers of opposite sign that may appear in Eq. (13) originally derived by A. Bar-Shalom et al. [9, 10]. The powerful method developed by F. Gilleron and J.C. Pain brings a considerable improvement to the implementation of the SC-approach, since it allows accurate calculation of partition functions at reasonable computer time even in the case of large supershells (e.g., when every Q-electron ion is represented by a single superconfiguration) and/or low temperatures.

As is well known [3], one of the principal problems to properly evaluate the contribution of bound ionic states to thermodynamic functions lies in appropriate modeling of their perturbation due to plasma environment. In dense plasma, ion-microfield perturbations lead to delocalization of the upper-shell electrons thus yielding a finite number of bound ionic states and providing convergence of the internal partition function.

In the present model, the effect of plasma microfields is incorporated into the partitions functions following the approach of D. Hummer and D. Mihalas [3, 7] through effective occupation probabilities of one-electron states of isolated ions. In particular, modified ion partition functions in the SC-approximation (currently, without first-order energy corrections $\overline{\Delta E_\Xi}$) are written as follows:

$$\widetilde{U}_Q\,(\rho, T, \mathbf{N}) = \sum_\Xi \widetilde{U}_\Xi, \quad \widetilde{U}_\Xi = \prod_{\sigma\in\,\Xi} \widetilde{U}_\sigma = \sum_{\sum_s q_s = Q_\sigma} \prod_{s\in\,\sigma} \binom{g_s}{q_s} \cdot \widetilde{X}_s^{q_s}, \tag{14}$$

$$\widetilde{X}_s = w_s^{(MF)}(\rho, T, \mathbf{N}) \cdot e^{-\beta\varepsilon_s}, \tag{15}$$

in which the following factors are introduced:

$$w_s^{(MF)}(\rho,T,\mathbf{N}) = \int_0^{\mathcal{E}_s^{(cr)}} P(\mathcal{E},\,\Gamma_e)\,d\mathcal{E}, \quad \mathcal{E}=\mathcal{F}/\mathcal{F}_0 \tag{16}$$

— occupation probabilities of one-electron states of an isolated ion including the effect of plasma microfields defined as the probabilities that the strength of microfield (which distribution is given by the function $P(\mathcal{E},\,\Gamma_e)$) does not exceed the value of critical electric field $\mathcal{E}_s^{(cr)} = \mathcal{F}_s^{(cr)}/\mathcal{F}_0$ for an s-shell (in the units of normal Holtsmark field $\mathcal{F}_0 = 2\pi\left(\frac{4}{15}\right)^{2/3} e\left(\langle\mathcal{Z}^{3/2}\rangle\rho N\right)^{2/3}$).

To model the effects of plasma microfields we adopted simple analytical expression for occupation probabilities derived in Ref. [7] with $\mathcal{F}_s^{(cr)} = K_n\varepsilon_s^2/4Z_s^{(eff)}e^3$ [3,7], where $Z_s^{(eff)}$ — effective ion charge seen by bound electrons on an s-shell, and K_n is the Stark-ionization correction factor (see [3]).

So, appropriately modified partition functions of supershells, comprising the SCs considered, can also be calculated with the recursive formulas of the SC-model [12].

Effective radii $\{R_Q\}$ of ions are found from the SCs yielding greatest contributions to modified ion partition functions that incorporate occupation probabilities of one-electron ion states in the presence of plasma electric microfields [7].

2.3 Modified Saha equations

Ionization balance **N** at LTE conditions with specific temperature and density values, corresponding to the minimal value of free energy $F\,(\rho,T,\mathbf{N})$ (Eq. (1)), can be obtained from the solution of modified Saha equations supplemented by the condition of electro-neutrality and conservation of nuclei in the ionization-recombination process $A^{\mathcal{Z}+} \rightleftharpoons A^{(\mathcal{Z}+1)+} + e^-$ [2,4]:

$$\begin{cases} \dfrac{c_Q}{c_{Q-1}} = \dfrac{\widetilde{U}_Q}{\widetilde{U}_{Q-1}}\cdot e^{\beta(\mu_e-\widetilde{\Delta\mu}_Q)}, \\ \\ \langle\mathcal{Z}\rangle = \dfrac{4}{\sqrt{\pi}}\dfrac{I_{1/2}(\beta\mu_e)}{\rho N\lambda_e^3} = K\cdot\dfrac{AT_{[\mathrm{keV}]}^{3/2}}{\rho_{[\mathrm{g/cm^3}]}}\;I_{1/2}(\beta\mu_e), \\ \\ \sum_Q(Z-Q)c_Q = \langle\mathcal{Z}\rangle, \quad \sum_Q c_Q = 1. \end{cases} \tag{17}$$

Here $c_Q = N_Q/N$ — Q-electron ion fraction; $\langle\mathcal{Z}\rangle = N_e/N$ — average ionization; $K = 357.785$; $\widetilde{\Delta\mu}_Q = \Delta\mu_Q - \Delta\mu_{Q-1} - \Delta\mu_e$ — excess chemical potential given by the difference of excess chemical potentials of particles involved in the ionization-recombination process [2,4]:

$$\widetilde{\Delta\mu}_Q = \left(\frac{\partial}{\partial N_Q} - \frac{\partial}{\partial N_{Q-1}} - \frac{\partial}{\partial N_e}\right)\Delta F - k_BT\sum_{Q'}\left(\frac{\partial}{\partial N_Q} - \frac{\partial}{\partial N_{Q-1}} - \frac{\partial}{\partial N_e}\right)\ln\widetilde{U}_{Q'}\,. \tag{18}$$

2.4 Equation of state

Once the total free energy $F\,(\rho,T,\mathbf{N})$ has been minimized, thermodynamic functions are obtained by direct differentiation of the total free energy. Thus, pressure P and specific internal energy E are given by [8]:

$$P\,(\rho,T,\mathbf{N}) = -\left(\frac{\partial F}{\partial V}\right)_{\mathbf{N},T} = \rho^2\left(\frac{\partial F}{\partial\rho}\right)_{\mathbf{N},\,T}, \quad E\,(\rho,T,\mathbf{N}) = -T^2\frac{\partial}{\partial T}\left(\frac{F}{T}\right)_{\mathbf{N},\,\rho}. \tag{19}$$

Accordingly to equations (1) and (19)

$$P\,(\rho,T,\mathbf{N}) = P_i^{(id)} + P_e^{(id)} + P_b + \Delta P, \tag{20}$$

$$E\,(\rho,T,\mathbf{N}) = E_i^{(id)} + E_e^{(id)} + E_{ioniz} + E_b + \Delta E, \tag{21}$$

where

$$P_i^{(id)} = \rho N k_B T,\ E_i^{(id)} = \frac{3}{2} N k_B T \tag{22}$$

are the ideal-gas ion contributions;

$$P_e^{(id)} = k_B T \frac{8}{3\sqrt{\pi}} \frac{I_{3/2}(\beta\mu_e)}{\lambda_e^3}, \quad E_e^{(id)} = k_B T \frac{4}{\sqrt{\pi}\rho} \frac{I_{3/2}(\beta\mu_e)}{\lambda_e^3} \tag{23}$$

are the ideal-gas contributions of (partially) degenerate free electrons;

$$E_{ioniz} = \sum_Q N_Q (1 - \delta_{Q,Z}) \sum_{k=0,\ Q \le Z-1}^{Z-Q-1} I_k \tag{24}$$

is the ionization energy (relative to the ground-state energy of isolated atom);

$$P_b = -\rho^2 k_B T \sum_Q N_Q \left(\frac{\partial \ln \widetilde{U}_Q}{\partial \rho} \right)_{\mathbf{N},\,T}, \quad E_b = k_B T^2 \sum_Q N_Q \left(\frac{\partial \ln \widetilde{U}_Q}{\partial T} \right)_{\mathbf{N},\,\rho} \tag{25}$$

are the bound-electron contributions to pressure and internal energy (excitation energy of ions);

$$\Delta P = \Delta P_C + \Delta P_{HS}, \quad \Delta E = \Delta E_C + \Delta E_{HS} \tag{26}$$

are the nonideality corrections allowing for Coulomb interaction of ions and electrons in the OCP-LMR approximation [5] (Eq. (4)) for multi-ionic mixture:

$$\Delta P_C = N k_B T \sum_Q c_Q \varepsilon_C(\Gamma)/3V, \quad \Delta E_C = N k_B T \sum_Q c_Q \varepsilon_C(\Gamma), \tag{27}$$

$$\varepsilon_C(\Gamma) = \Gamma^{3/2} \left[\frac{A_1}{\sqrt{\Gamma + A_2}} + \frac{A_3}{\Gamma + 1} \right] + \frac{B_1 \Gamma^2}{\Gamma + B_2} + \frac{B_3 \Gamma^2}{\Gamma^2 + B_4}. \tag{28}$$

and finite-ion-volume corrections as given by the hard-sphere model [17] (Eq. (6)):

$$\Delta P_{HS} = \rho N k_B T \eta \frac{\partial f_{HS}}{\partial \eta}, \quad \Delta E_{HS} = -N k_B T^2 \frac{\partial f_{HS}}{\partial \eta} \cdot \frac{\partial \eta}{\partial T}. \tag{29}$$

3 Results

Using the CP-representation, we calculated ionization equilibrium and thermodynamic properties of dense Al and Fe plasmas.

An accurate modeling of ionization equilibrium is essential for calculating plasma EOS, transport coefficients, and optical properties. Figure 1 presents calculated average ionization $\langle \mathcal{Z}(\rho/\rho_0) \rangle$ of aluminum ($\rho_0 = 2.7$ g/cm^3) (a) and iron ($\rho_0 = 7.85$ g/cm^3) (b) plasmas along isotherms $T = 0.03,\ 0.3$ and 3 keV compared to the calculations performed with the Thomas-Fermi model (interpolation formula of R.M. More [18]) and the modified Hartree-Fock-Slater (MHFS) average-atom model [19]. Our results appear to be in an overall agreement with those from the Thomas-Fermi and MHFS models. It is seen that all three models predict the increase of $\langle \mathcal{Z} \rangle$ near the solid density at the lowest temperature considered thus demonstrating the pressure ionization but with the noticeably different values of the effect in the domain of dense partially ionized plasmas.

Figure 2 shows the LTE ion-fraction distributions in Al and Fe plasmas calculated with the present CP-model at temperatures of 0.03 keV and 0.3 keV and densities $\rho/\rho_0 = 0.01,\ 1$ and 5. Here one can clearly see the shift of the ionization equilibrium due to pressure ionization as the density increases from $\rho/\rho_0 = 1$ to $\rho/\rho_0 = 5$.

Calculated thermodynamic functions allow us to compare the values of Grüneisen coefficient defined as the ratio of thermal pressure to thermal energy density $\gamma = P/(\rho E)$. Calculated Grüneisen coefficients of the Al (a) and Fe (b) plasmas along the isochores $\rho/\rho_0 = 0.01,\ 1$ and 5 are presented in Figure 3. Our results are compared

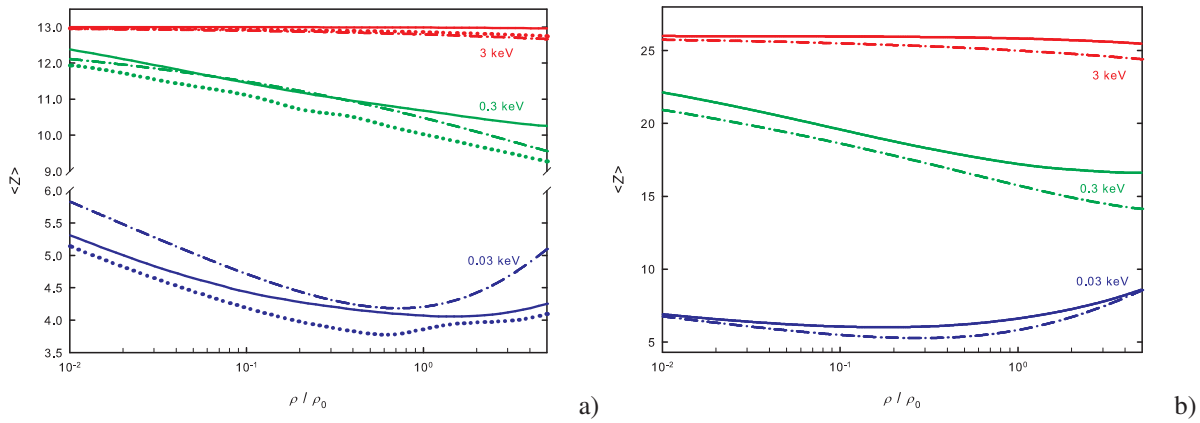

Fig. 1 Average ionization of Al (a) and Fe (b) plasmas along isotherms $T = 0.03,\ 0.3$, and 3 keV calculated with the present CP-model (solid), Thomas-Fermi [18] (dash-dotted), and MHFS (dotted) [19] models.

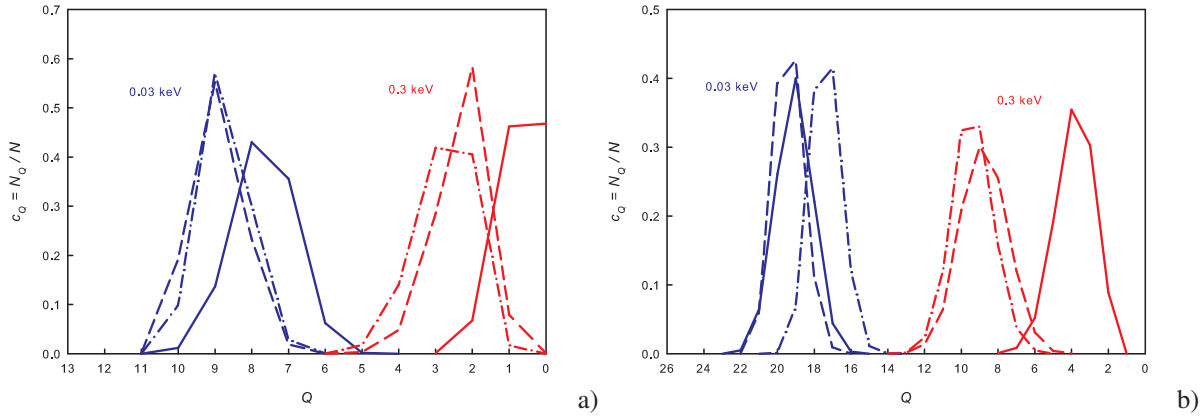

Fig. 2 Ionization distribution of Al (a) and Fe (b) plasmas calculated with the present CP-model at temperatures $T = 0.03$ and 0.3 keV and densities $\rho/\rho_0 = 0.01$ (solid lines), 1 (dashed lines), 5 (dash-dotted lines).

to the calculations performed with an improved Thomas-Fermi TFPK model [20] and the MHFS model [19]. As expected, the TFPK model smooths the manifestation of the shell structure of ions while the present model and MHFS both reveal shell oscillations due to ionization of K-, L-, and M-(for Fe) shell electrons. One can also see that shell oscillations along the isochores get smoothed and shifted into the high-temperature region at higher plasma densities due to the plasma effects. Here, the positions of local peaks in γ (in the region of each shell oscillation) along the isochores correspond to $\partial\langle\mathcal{Z}\rangle/\partial T \simeq 0$, i.e. to the completion of ionization of relevant shell and beginning of ionization of deeper electron shells.

Figure 4 (a) shows calculated Hugoniots for the solid-density aluminum along with the experimental [21–25] and other theoretical data. The latter were obtained by the TFPK model [20] and by the MHFS [19] and ESODE ("Atom-in-Cell") [26] models taking into account ionic shell structure. Significant experimental errors for the shock compressed aluminum in the pressure region of $P \simeq 40 - 240$ Mbar in the experiment [21] were later reduced [23] by using some improvements in the experimental setup and the measurement procedure. One can see that the MHFS, ESODE, and the present model predict well-pronounced closely matching shell oscillations at the pressures $P = 10^2 - 10^4$ Mbar due to ionization of the L- and K-shell electrons while the TFPK model, as expected, smooths those and represents the details of shock Hugoniot only on the average. On the other hand, the experimental error bars relevant to the ultrahigh-pressure region of $P \simeq 10^2 - 10^4$ Mbar for the shock compressed aluminum are too large to experimentally evaluate the amplitude of the shell oscillations and thus conclude which theoretical model better fits the experimental data.

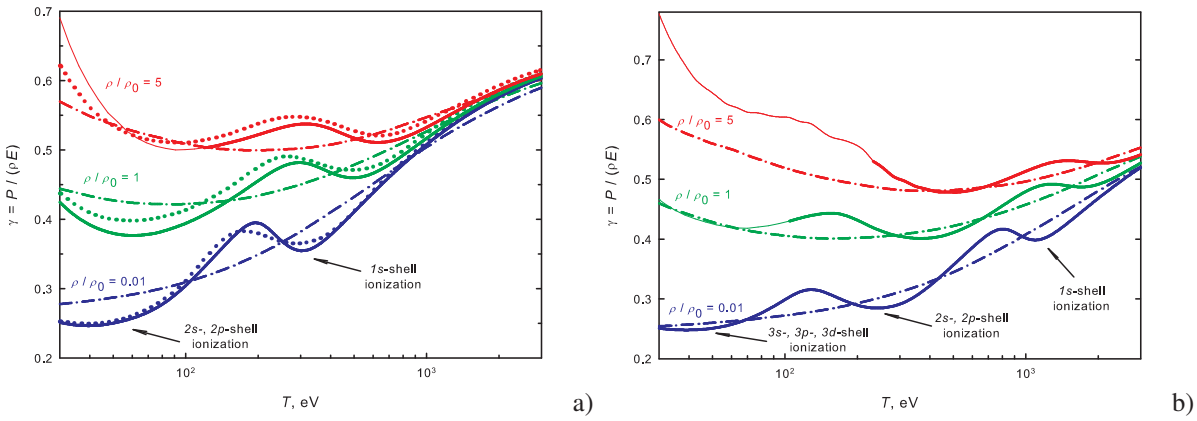

Fig. 3 Grüneisen coefficient of Al (a) and Fe (b) plasmas along isochores $\rho/\rho_0 = 0.01,\ 1$ and 5. Solid — present CP-model; dash-dotted — improved Thomas-Fermi TFPK model [20]; dotted — MHFS [19]. Lines marked in thin-solid correspond to the temperature regions where nonideality corrections to the ideal-gas contributions in the present EOS appear to be greater than 30 %.

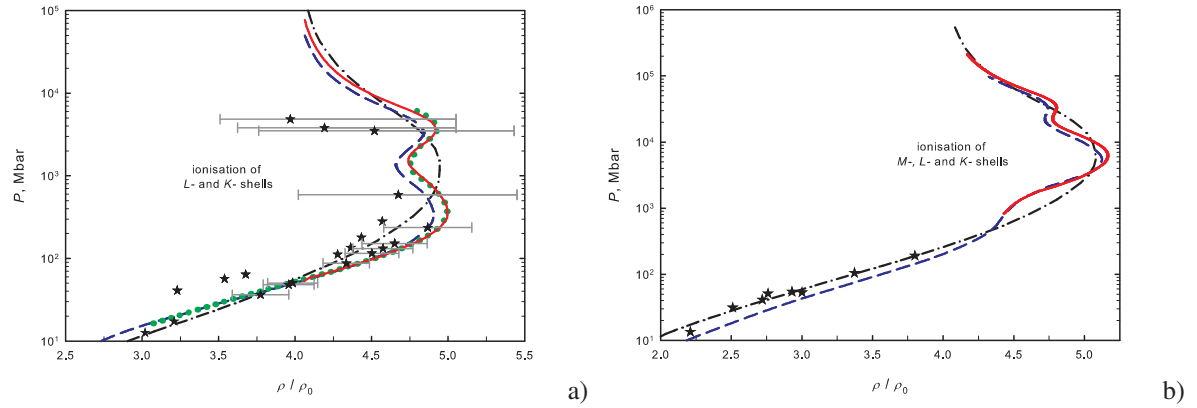

Fig. 4 Comparison of Hugoniots for the solid-density Al (a) and Fe (b) calculated with the present model (red, solid) and various cell models (TFPK [20] (black, dash-dotted), MHFS [1] (green, dotted), and ESODE (ASC) [26] (blue, dashed)) to the experimental data [21–25] (symbols).

It is also seen that along with the MHFS and ESODE data, our calculations provide fairly good description of experimental shock compressibility of solid Al [23] at the pressures $P \simeq 40 - 240$ Mbar. Such pressures correspond to the density, temperature, and (specific) internal energy values $\rho/\rho_0 \simeq 4 - 5$, $T \simeq 0.025 - 0.08$ keV and $E \simeq 0.5 - 3.6$ MJ/g, respectively, typical for the high-density region of the WDM domain.

Comparison of Hugoniots for the solid-density iron calculated with the present model and ion-cell models TFPK and ESODE is shown in Figure 4 (b). In this case, Hugoniot curve has three shell oscillations at the pressures $P = 3 \cdot 10^2 - 4 \cdot 10^4$ Mbar due to ionization of M-, L- and K-shell electrons. As in the aluminum case, the Hugoniot for solid-density iron calculated with the present model reveals good agreement with the ion-cell models. At the same time, our results are found to be more close to the ESODE data then in the case of Al. This may be due to the fact that the approximation used to calculate occupation probabilities does not allow for the electron-degeneracy effects, lowering the plasma nonideality, and thus underestimates the truncation of ion excited states that would be more pronounced at lower Coulomb screening because of smaller values of integrals over the microfield distribution function in $w_s^{(MF)}$ (Eq. (16)). Since in the region of the L-shell ionization the value of the degeneracy parameter $n_e\lambda_e^3 \approx 1$ and 0.2 for Al and Fe, respectively (mostly due to higher temperature $T \approx 0.5$ keV versus $T \approx 0.1$ keV for Al plasmas), disregarded electron degeneracy in calculated occupation probabilities may yield somewhat better description in the case of the Fe plasmas considered.

It is also worth comparing electronic specific heat per particle along the Hugoniot curve which is defined as:

$$C_v^{(e)} = \frac{1}{3Nk_B/2}\frac{\partial[E(\rho,T) - E_i(\rho,T)]}{\partial T}, \tag{30}$$

where $E_i(\rho,T) = 3/2\ Nk_BT + Nk_BT\sum_Q c_Q\,[\varepsilon_c(\Gamma) - A_1\Gamma]$.

Figure 5 shows calculated electronic specific heat per particle $C_v^{(e)}$ along the Hugoniot curve for solid-density aluminum and iron. The result calculated with the present CP-model is found to be in a good qualitative and quantitative agreement with the ESODE data [26] up to $T \simeq 25$ eV — strongly-coupled plasma domain (lines marked in thin-solid) where ion and electron coupling parameters take the values $\Gamma > 10$, $\Gamma_e > 2$, respectively, and nonideality corrections to the ideal-gas contributions in the EOS become greater than 30 %.

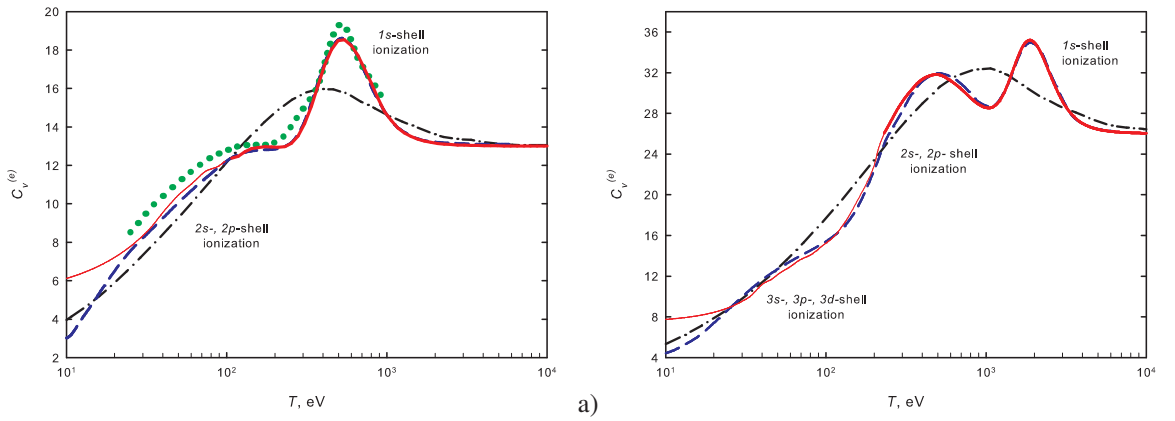

Fig. 5 Electronic specific heat per particle along the Hugoniot curve for Al (a) and Fe (b). Present model — red, solid and long-dashed; TFPK [20] — black, dash-dotted; ESODE (ASC) [26] — blue, medium-dashed; MHFS [1] — green, dotted. Lines marked in thin-solid correspond to the present CP-model data for which nonideality corrections to the ideal-gas contributions in the EOS functions appear to be greater than 30 %.

4 Conclusions

Using the chemical-picture approach, we have performed the modeling of thermodynamic properties of dense multicharged-ion plasmas at temperatures 0.03–3 keV and densities $10^{-3} - 5$ of their normal material densities. Theoretical model involves the effects of Coulomb non-ideality (generalization of OCP liquid of classical ions for multi-ionic mixture) and degeneracy of plasma electrons, contribution of bound ion states with the employment of the modified superconfiguration approximation, and hard-sphere-model representation of the finite-volume effects of plasma ions.

Even at high density values $\rho \geq \rho_0$ of aluminum and iron plasmas, the present model shows fairly good agreement for thermodynamic functions and shock Hugoniots with the theoretical data given by the MHFS [1,19] and ESODE (ASC) [26] average-atom models taking into account ionic shell structure. The agreement of our results with an improved Thomas-Fermi TFPK model that essentially smooths the details of the shell structure of plasma ions is found to be reasonable, on the average.

Currently, the CP model presented is being extended and improved to more appropriately describe Coulomb interaction (on the base of the multicomponent hypernetted-chain approach [27]) and finite-ion-volume effects at strong plasma coupling, implementation of a flexible and temperature dependent atomic-shell-to-supershell gathering algorithm, and more accurate modeling of occupation probabilities.

Acknowledgements The work has been supported in part by the International Science and Technology Center under the project Nr. 3755.

References

[1] A.F. Nikiforov, V.G. Novikov, and V.B. Uvarov. *Quantum-Statistical Models of Hot Dense Matter. Methods for Computation Opacity and Equation of State*. Birkhäuser, Basel, Switzerland 2005.

[2] V.K. Gryaznov, I.L. Iosilevsky, V.E. Fortov. *Thermodynamic properties of shock-compressed plasmas represented with the chemical-picture model*. Shock waves and Extreme States of Matter. Nauka, Moscow, 2000 [in Russian].

[3] D.G. Hummer, D. Mihalas. Astrophys. J., **331**, 794 (1988).

[4] P. Hakel, D.P. Kilcrease. *CHEMEOS: A New Chemical-Picture-Based Model for Plasma Equation-of-State Calculations*. Proc. of the 14^{th} APS Topical Conference on Atomic Processes in Plasmas, Santa Fe (2004).

[5] G. Chabrier, A. Potekhin, Phys. Rev. E, **58**, 4941 (1998);
G. Chabrier, A. Potekhin, Phys. Rev. E, **62**, 8554 (2000).

[6] G.A. Mansoori, et al. J. Chem. Phys., **54**, 1523 (1971).

[7] A. Nayfonov, W. Däppen, D. Hummer, D. Mihalas. Astrophys. J., **526**, 451 (1999).

[8] L.D. Landau, E.M. Lifshitz. *Statistical Physics*, Pt. I (Pergamon, Oxford, 1986).

[9] A. Bar-Shalom, et al. Phys. Rev. A, **40**, 3183 (1989).

[10] J. Oreg, A. Bar-Shalom, M. Klapisch. Phys. Rev. E, **55**, 5874 (1997).

[11] O. Peyrusse. J. Phys. B: At. Mol. Opt. Phys. **33**, 4303 (2000).

[12] F. Gilleron, J.C. Pain. Phys. Rev. E, **69**, 056117 (2004).

[13] R.D. Cowan. *The theory of atomic structure and spectra*. UC. Press, Berkeley, Los Angeles, London (1981).

[14] H.E. DeWitt, W. Slattery, G. Chabrier. Physica B, **228**, 158 (1996).

[15] H.E. DeWitt, W. Slattery. Contrib. Plasma Phys., **39**, 97 (1999).

[16] H.E. DeWitt, W. Slattery. Contrib. Plasma Phys., **43**, 279 (2003).

[17] N.F. Carnahan, K.E. Starling. J. Chem. Phys., **51**, 635 (1969).

[18] R.M. More. Adv. At. Mol. Phys., **21**, 305 (1985).

[19] A.F. Nikiforov, V.G. Novikov, S.K. Truhanov, V.B. Uvarov. VANT, Ser. Metodiki i Programmy ... (Methods and programs ..., **3**, 62 (1990) [in Russian].

[20] N.N. Kalitkin, L.V. Kuzmina. *Thermodynamic functions of matter at high energy density*. Preprint of M.V. Keldysh Insitute of Applied Mathematics No. 35 (1975) [in Russian];
V.P. Kopyshev. Chislennye Metody Mekhaniki Sploshnoj Sredy (Numerical methods of continuum mechanics), **8**, 54 (1977) [in Russian].

[21] A.S. Vladimirov, N.P. Voloshin, V.N. Nogin, et al. JETP Lett., **39**, 82 (1984).

[22] V.A. Simonenko, N.P. Voloshin, A.S. Vladimirov, et al. Sov. Phys. JETP, **61**, 869 (1985).

[23] E.N. Avrorin, B.K. Vodolaga, N.P. Voloshin, and V.F. Kuropatenko. JETP Lett., **43**, 308 (1986);
E.E. Mironova and A.T. Sapozhnikov. *Equation of state of aluminum allowing for evaporation and ionization*. Abstr. of Intl. conf.: VIII Zababakhin scientific talks, Snezhinsk, September 8–12, 2003, p. 190.

[24] M.A. Podurets, V.M. Ktitorov, R.F. Trunin, et al. Teplofiz. Vys. Temp. (Thermophysics of High Temperatures), **32**, 952 (1994) [in Russian].

[25] A.V. Bushman, I.V. Lomonosov, K.V. Khischchenko. *Shock Wave Database* and references therein, *http://teos.ficp.ac.ru/rusbank/*.

[26] J.C. Pain. Contrib. Plasma Phys, **47**, 421 (2007).

[27] K. Wünsch, J. Vorberger, and D.O. Gericke. Phys. Rev. E, **79**, 010201 (2009).